

# The Environmental Acoustics of Two Alaskan Rivers and Its Relation to Salmon Counting Sonars

by

Peter H. Dahl, *Applied Physics Laboratory, University of Washington, Seattle, Washington*

Harold J. Geiger & Deborah A. Hart, *Alaska Department of Fish and Game, Juneau, Alaska*

James J. Dawson, *Biosonics, Inc., Seattle, Washington*

Sam V. Johnston, *Hydroacoustics Technology, Inc., Seattle, Washington*

Donald J. Degan, *Aquacoustics, Inc., Kenai, Alaska*

Technical Report

**APL-UW TR 2001**

August 2000

*ADF&G Contract IHP-98-003*

*20000922 023*

**20000922 023**

## ACKNOWLEDGMENTS

This study was supported by the Alaska Department of Fish and Game under contract IHP-98-003. The study could not have been completed without the critical, and enthusiastic, assistance and input from Deborah Burwen, Dan Bosch, Jim Edmundson, Jim Miller, Steven Fleischman, and Carl Pfisterer, all from the Alaska Department of Fish and Game, Dave Daum from the U. S. Fish and Wildlife Service (Fairbanks), and Dr. Steven Kargl from the Applied Physics Laboratory.

## ABSTRACT

During the summer of 1999, the Applied Physics Laboratory worked with the Alaska Department of Fish and Game, Biosonics Inc., and Hydroacoustics Technology Inc. to make underwater environmental acoustic measurements in Alaska's Kenai and Wood rivers. The goal of these measurements was to understand, and model, the sources and magnitude of background acoustic reverberation, defined as the average acoustic intensity versus time (range) in the absence of any scattering from fish. The background reverberation determines, in part, the minimum size class of fish detectable and the accuracy of fish-tracking and counting algorithms that exploit the complex phase of the fish echo. It is also necessary to establish rigorous detection probabilities for all fish size classes. This report summarizes the results and analysis of these measurements and presents environmental acoustic models that can be used to evaluate signal-processing and fish-tracking algorithms.

## CONTENTS

<b>EXECUTIVE SUMMARY</b> .....	vii
<b>1. INTRODUCTION</b> .....	1
<b>2. MEASUREMENTS IN THE KENAI RIVER</b> .....	3
2.1 Site Description and Geometry .....	3
2.2 Acoustic Measurements .....	5
2.3 Reverberation Due to Volume Scattering .....	7
2.4 Reverberation Due to Bottom Backscattering .....	12
<b>3. MEASUREMENTS IN THE WOOD RIVER</b> .....	16
3.1 Site Description and Geometry .....	16
3.2 Acoustic Measurements .....	17
<b>4. SUMMARY AND CONCLUSIONS</b> .....	22
<b>REFERENCES</b> .....	25
<b>APPENDIX, Comparative Measures of Scattering from Bubbles and Glacial Silt Particles and a Model Relating Turbidity Measures to Volume Scattering from Glacial Silt Particles</b> .....	A1

## LIST OF FIGURES

Figure 1.	Map of the lower Kenai River showing location of the sonar test site .....	3
Figure 2.	Experimental geometry for acoustic reverberation measurements made in the Kenai River and key geometric variables .....	4
Figure 3.	Results of the CTD measurements made in the Kenai River at 1030 local time on 8 June 1999 .....	5
Figure 4.	Image of 100 pings transmitted at 1-s intervals and a frequency of 420 kHz versus ping number and range from sonar; reverberation level from ping number 33, mean $RL$ based on the 100-ping ensemble average, and a model for $RL$ .....	9
Figure 5.	Mean $RL$ at 200 kHz versus range from sonar based on a 100-ping ensemble average and a model for $RL$ .....	10
Figure 6.	Sample histogram of the ping-by-ping 420-kHz reverberation level corresponding to a range of 15 m in the data shown in Figure 4 ..	11
Figure 7.	The geometry of backscattering from a sloping riverbed .....	13
Figure 8.	Mean $RL$ measured at 200 kHz versus range from sonar based on 100-ping ensemble average; model for $RL_v$ ; model for $RL_b$ , and the incoherent sum of $RL_v$ and $RL_b$ .....	14
Figure 9.	Mean $RL$ measured at 420 kHz versus range from sonar based on 100-ping ensemble average; model for $RL_v$ ; model for $RL_b$ , and the incoherent sum of $RL_v$ and $RL_b$ .....	15
Figure 10.	Map of the Wood River showing the location of the sonar test site .....	16
Figure 11.	Experimental geometry for the acoustic reverberation measurements made in the Wood River and key geometric variables .....	17
Figure 12.	Mean $RL$ measured at 200 kHz versus range based on a 100-ping ensemble average, and a model for $RL$ .....	18
Figure 13.	Mean $RL$ measured at 420 kHz versus range based on a 100-ping ensemble average for $\theta_P = 0^\circ$ and $\theta_P = 8^\circ$ , and a model for $RL$ .....	19

Figure 14. Sample histogram of the ping-by-ping 420-kHz reverberation level corresponding to the data shown at a range of 5 m in Figure 13 ..... 20

Figure A1. Backscattering cross section,  $\sigma_{bs}$ , for a single bubble or particle of glacial silt versus bubble or particle radius,  $a$ , for acoustic frequencies of 420 kHz and 200 kHz ..... A1

## EXECUTIVE SUMMARY

During the summer of 1999, the Applied Physics Laboratory, along with the Alaska Department of Fish and Game, Biosonics Inc., and Hydroacoustics Technology Inc., conducted sonar measurements in Alaska's Kenai and Wood rivers. The goal of these measurements was to gain an understanding of, and model, the sources and magnitude of background acoustic reverberation. Background reverberation is defined as the average acoustic intensity versus time (range) in the absence of any scattering from fish. The background reverberation determines, in part, the minimum size class of fish detectable and the accuracy of fish-tracking and counting algorithms that exploit the complex phase of the fish echo. In addition, it is necessary to establish rigorous detection probabilities for fish of all size classes. The measurements were at 200 kHz and 420 kHz, in conditions and geometries that simulated the configuration used by sonars for counting fish in rivers. These measurements produced estimates of the reverberation level ( $RL$ ) (in dB re  $\mu\text{Pa}$ ) and estimates of the variance of this quantity.

There are two primary sources of reverberation, scattering by particles and bubbles entrained in the water volume (*volume scattering*) and scattering from the riverbed (*bottom scattering*). Our study shows that volume scattering is the more important of these two contributions, and it can be described by the *scattering strength* ( $S_v$ ) in decibels.

For the Kenai River site, we estimated  $S_v$  to be  $-67 \text{ dB} \pm 4 \text{ dB}$  at 200 kHz and  $-53 \text{ dB} \pm 4 \text{ dB}$  at 420 kHz. The difference is predicted by the frequency-to-the-fourth-power law associated with Rayleigh scattering. For the Wood River site, Rayleigh scattering also applies, and we estimate  $S_v$  to range from  $-55 \text{ dB}$  to  $-66 \text{ dB}$  at 200 kHz and from  $-42 \text{ dB}$  to  $-53 \text{ dB}$  at 420 kHz; this larger range is associated with tidally influenced river currents which modulate the bubble density. We also modeled fluctuations in  $RL$  and demonstrated that at a fixed range and under stationary conditions, fluctuations in  $RL$  and  $S_v$  are well described by the probability density function (PDF) given by Eq. (5) in Section 2.3.

A model developed from this study for  $S_v$  caused by scattering from suspended glacial silt particles (and thus applicable to the Kenai River) is presented in the appendix. The predictions of the model agree well with our estimates of  $S_v$ , but the effect of possible additional scattering from bubbles needs to be determined. This model should, however, motivate further study on the relationship between  $S_v$  and turbidity, and it may be particularly useful for acoustical-limnological studies in Alaskan lakes containing glacial meltwater.

Our study quantifies how using horizontal-looking sonars to detect fish in rivers is reverberation limited and not noise limited. Knowing  $S_v$ , for example, we can then estimate the minimum target strength of fish,  $TS_{\min}$ , that can be reliably detected. Assuming, for example, that  $TS_{\min}$  must be at least 10 dB more than the equivalent target strength of the volume of water ensonified,  $TS_{\text{vol}}$ , then it follows that  $TS_{\min} \geq TS_{\text{vol}} + 10$  dB, where

$$TS_{\text{vol}} = 10 \log_{10} \left( \frac{c\tau}{2} R^2 \psi \right) + S_v.$$

This equation can be used to evaluate the impact of changing the pulse length,  $\tau$ , of the sonar beam as parameterized by  $\psi$ , and range,  $R$ , with respect to fish-detection goals and algorithms.

Another important estimate that depends on  $S_v$  is the root mean square (rms) error in angular location,  $\theta_{\text{rms}}$ , when tracking fish with split-beam sonars. This error is proportional to  $\frac{1}{\sqrt{\text{SNR}}}$ , where SNR is the signal-to-reverberation ratio and is determined by

$$\text{SNR} = 10^{(TS_{\text{fish}} - TS_{\text{vol}})/10},$$

where  $TS_{\text{fish}}$  is the nominal target strength of a fish at side aspect.

# 1 INTRODUCTION

In several important commercial, and sport, fishing salmon river systems, the Alaska Department of Fish and Game (ADF&G) uses side-looking sonars mounted along riverbanks to count adult salmon during their upstream migration. During the 1990s, the average commercial catch of Pacific salmon in Alaska was 175 million fish; the commercial catch exceeded 215 million fish twice in that decade. High harvest levels of Pacific salmon from the mid 1970s to the present have been maintained by a combination of careful, active management [1] and favorable environmental conditions [2],[3]. In most cases, the harvests have been managed to achieve approximately fixed spawning stock sizes that do not change with year-to-year variation in abundance. A major technical challenge has been to estimate spawning stock size while the runs and the fisheries are actively under way. Some runs last just a few weeks and involve tens of millions of adult salmon moving into vast, remote wilderness areas to spawn. The fisheries managers can visually estimate or monitor passage with aerial observations, counting towers, or counts through weirs for systems with clear water. Sonar has been used since the 1960s for important spawning systems in Alaska that are glacially influenced or otherwise not suitable for visual observation [4],[5]. Early studies involved arrays of up-looking sonar produced by the Bendix Corporation. By 1965 engineers from Bendix tested a side-looking design that formed the basis of the machines that are still used in many important salmon-producing rivers in Alaska. In 1997, the Alaska Department of Fish and Game decided to replace the 1960s vintage sonars with split-beam systems. Field tests of side-looking split-beam sonar began in 1998 and continued in 1999.

This report summarizes results of a project involving the Applied Physics Laboratory (APL), ADF&G, Biosonics Inc., and Hydroacoustics Technology Inc. (HTI) to measure, and model, the background acoustic reverberation in two Alaskan rivers. Background reverberation is defined as the average acoustic intensity of the echo versus time (range) in the absence of any contribution from fish. The rivers were the Kenai River, located on the Kenai Peninsula, and the Wood River, which drains into Bristol Bay near Dillingham. The measurements were made at two frequencies: 420 kHz, using a system built by Biosonics Inc., and 200 kHz, using a system built by HTI. For each system, a combination of transducers and pulse lengths was employed as discussed in the following sections.

Background reverberation determines, in part, the minimum size class of fish that is detectable with sonar and the accuracy of fish-tracking and counting algorithms that use the complex phase of the fish echo, and is necessary to establish rigorous detection probabilities for all fish size classes. Furthermore, with a reasonably accurate model for background reverberation, it is possible to simulate the acoustic background to

evaluate the consequences of a change in sonar system parameters such as pulse length, transducer beamwidth, or frequency on fish-detection and tracking algorithms. We determined that the background reverberation in both riverine environments studied was set by, in order of importance, (1) scattering from bubbles and particles of glacial silt entrained in the water column (*volume backscattering*), and (2) scattering from the rough surface of the riverbed (*bottom backscattering*).

The report is organized as follows. Section 2 summarizes the measurements made at the Kenai site and the resulting sonar models for background reverberation, and Section 3 repeats this summary for the Wood River site. Note that Section 2 is considerably longer than Section 3 as it includes introductory remarks and a discussion of important notation used throughout the report. In Section 4 we summarize and present conclusions, and in the appendix we present a model for volume scattering from glacial silt that applies to the Kenai River.

## 2 MEASUREMENTS IN THE KENAI RIVER

### 2.1 Site Description and Geometry

The Kenai River measurements were made 8 and 9 June 1999 at a site 8.5 miles upstream from the mouth of the river (Fig. 1) on the right bank that is used by ADF&G for sonar counting of migrating chinook salmon (*Oncorhynchus tshawytscha*). The Kenai River at this site is approximately 90 m wide and 5 m deep at the thalweg at mean tide level; the river depth undergoes a tidal fluctuation of approximately  $\pm 1.5$  m. Additional details concerning this site are available in Refs. 6 and 7. The HTI system was located about 50 m upstream from the ADF&G sonar counting site, and the Biosonics system was located another 10 m upstream from the HTI system. Fathometer readings were made from cross-river transects at both locations the day before measurements started. These data were used to construct a bathymetric profile of the right bank of the Kenai River, starting from each transducer location. Figure 2, for example, shows the position of the Biosonics transducer along with important geometric variables, which are the transducer's height above the bottom,  $H_T = 0.48$  m, the average bottom slope,  $\theta_S$ , and the water depth,  $D$ , versus range,  $R$ , from the sonar. At the Biosonics location the bottom slope varied from about  $4^\circ$  just out from the transducer to about  $3^\circ$  at a range of 20 m, with  $3.5^\circ$  representing a nominal average slope of the riverbed. The fathometer readings made at the HTI

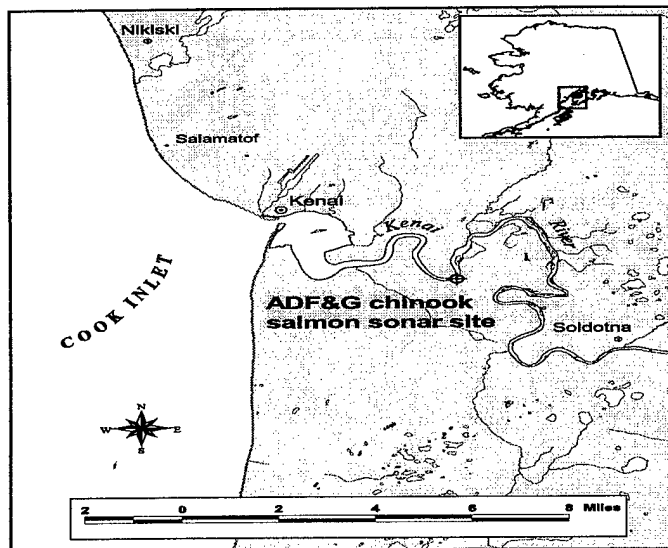
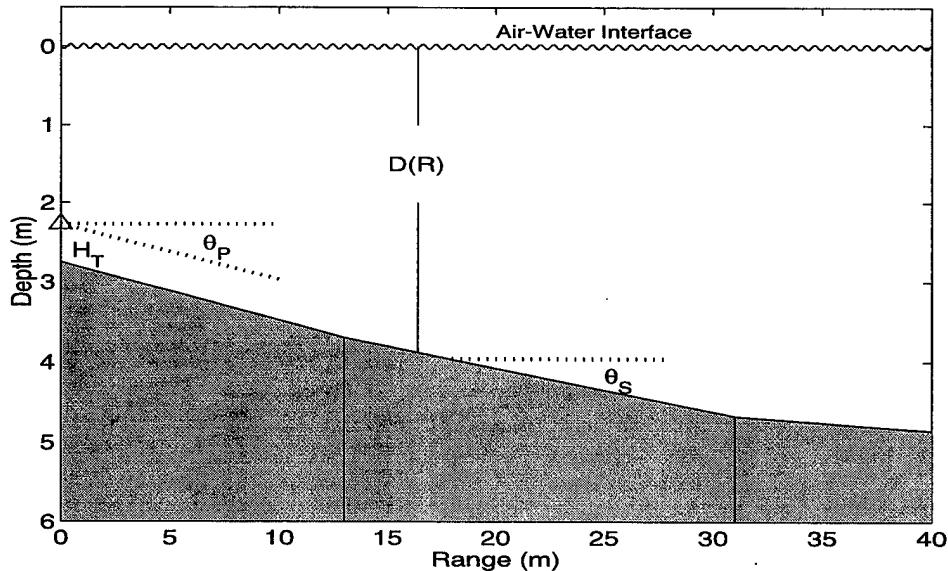


Figure 1. Map of the lower Kenai River showing location of the sonar test site.



**Figure 2.** Experimental geometry for acoustic reverberation measurements made in the Kenai River and key geometric variables. View represents a portion of the river cross section at its right bank extending out to the thalweg corresponding to the location of the Biosonics system. The transducer's position is shown by the large triangle at range = 0 m. The bottom contour has been constructed from fathometer readings made during cross-river transects.

location showed a similar bathymetry, but the average slope across the transect was closer to  $3^\circ$ ; also, for the HTI system  $H_T = 0.25$  m. Note that  $D$  changed over the time period (approximately 3 hours) during which the acoustic measurements were made owing to tidal effects. We obtained the correct  $D$  at the time of each acoustic measurement from depth measurements made by ADF&G personnel at their sonar site.

Because the Kenai River undergoes tidal fluctuations at the experimental site, it was important to first evaluate the effect, if any, of these fluctuations on the acoustic environment. Specifically, it is possible that an incoming tidal flow could transport with it high-salinity seawater that would mix with the less saline river water, increasing both the acoustic attenuation and the sound speed. To evaluate this, several conductivity-temperature-depth (CTD) measurements were made with a Sea-Bird CTD unit on 7 and 8 June to sample various tidal phases. Figure 3 shows the results of a CTD measurement made at 1030 on 8 June, which is representative of the other measurements. (Note: All times reported here are local.) The three types of lines represent CTD deployments made at three points roughly evenly spaced across the river. The dotted-dashed line corresponds to readings closer to the right bank; the solid line corresponds to readings near the thalweg, and therefore extends the deepest;

the dashed line corresponds to readings closer to the left bank. The measurements show that (1) salinity was extremely low (approximating fresh water), and (2) the sound speed was primarily determined by water temperature, which was nearly constant with depth. During this particular measurement the water temperature was about 8.25°C, but for others the temperature ranged between 8° and 9°C, which puts the sound speed,  $c$ , in the range 1438.5 m/s to 1442.6 m/s [8]. No salinity of any acoustic significance was measured, and thus the main effect of the tide on the acoustic environment was to vary the water depth,  $D$ .

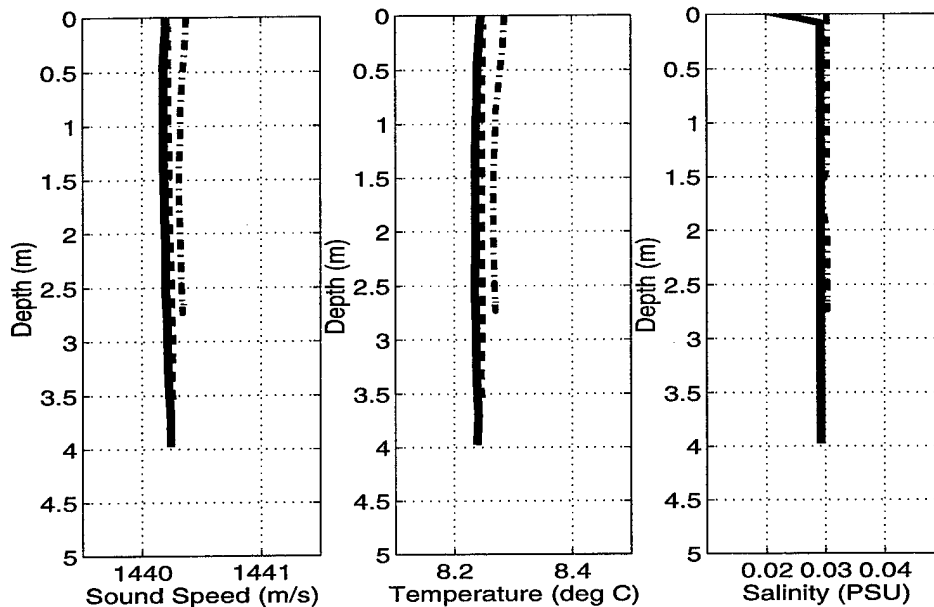


**Figure 3.** Results of the CTD measurements made in the Kenai River at 1030 local time on 8 June 1999. Dotted-dashed line is the measurement made approximately 20 m out from the right bank, the solid line is the measurement made near the thalweg, and the dashed line is the measurement made approximately 20 m out from the left bank. The salinity is displayed here in practical salinity units, or PSU.

## 2.2 Acoustic Measurements

One of the key objectives of the 1999 field effort on the Kenai and Wood rivers was to study sonar fish-tracking and enumeration strategies using the Biosonics and HTI systems. This report focuses only on the environmental acoustic measurements made with these two systems in order to understand background reverberation in sonar-based fish counting. However, a protocol had to be designed to measure acoustic reverberation in a convenient manner while also utilizing the optimum positioning of

the two sonars for fish detection. This protocol, which was also followed during the Wood River measurements, is outlined below.

Each operator determined the optimum transducer pitch angle,  $\theta_P$  (defined as positive downward), for counting fish at their particular site. Typically, the transducers need to be aimed downward a few degrees from horizontal such that the main lobe of the transducer beam is placed within the path of the migrating salmon. The salmon swim within a few centimeters of the riverbed to take advantage of the reduced water velocity within the bottom boundary layer [9]. The final established pitch angle, call it  $\theta_P = \theta_{PF}$  for *fish angle*, is influenced by the transducer's beamwidth, the bottom slope, and the composition and granularity of the riverbed. The operator selects  $\theta_{PF}$  by increasing  $\theta_P$  until the ensuing backscatter from the riverbed increases significantly and begins to dominate the background reverberation. At this point  $\theta_P$  is reduced perhaps a degree or two (i.e., back toward the horizontal) with subsequent reduction in the background reverberation. Once  $\theta_{PF}$  was established, background acoustic reverberation measurements were made at this angle and at various pitch angles above and below  $\theta_{PF}$ . For the Biosonics system  $\theta_{PF}$  was determined to be  $4^\circ$ ; the  $\theta_P$  settings used for the acoustic measurements included this angle as well as  $-2^\circ$ ,  $0^\circ$ ,  $5^\circ$ , and  $8^\circ$ . For the HTI system  $\theta_{PF}$  was determined to be  $2^\circ$ , and the  $\theta_P$  settings included this angle,  $0^\circ$ , and  $4^\circ$ . (The transducer pitch angles reported here are to the nearest degree.)

A measurement was defined as 100 pings transmitted at 1-s intervals. Upon completion of a measurement, the data were examined briefly, and then the measurement was repeated using a different  $\theta_P$  or pulse length,  $\tau$ . For the 420-kHz system, measurements were made at  $\tau = 0.2$  ms and 0.4 ms. For the 200-kHz system, measurements were made at  $\tau = 0.2$  ms and 0.5 ms and with an FM pulse with a bandwidth of 10 kHz and an effective pulse length of 0.18 ms. Other key sonar system parameters used during the Kenai measurements (which are discussed in the text) are summarized in Table 1.

**Table 1.** Sonar system parameters used for acoustic measurements in the Kenai River.

System	Frequency (kHz)	Source Level (dB)	$\phi_W$ (deg)	$\phi_N$ (deg)	$10 \log_{10} \psi$ (dB)
Biosonics (circ.)	420	216.1	2.3	2.3	-30.4
HTI (ellip.)	200	217.6	10.1	2.3	-24.0

## 2.3 Reverberation Due to Volume Backscattering

Volume reverberation is the term used to describe the scattering of sound back toward the transducer from the total volume of water ensonified by the sonar pulse. Here we introduce important notation used in both the analysis and the reporting of results. The discussion follows closely the one given by Dahl [8].

Consider a cloud of scatterers at range  $R$  corresponding to the cloud's center. If we ignore for now the loss due to sound attenuation in water, an elemental volume,  $dV$ , produces a backscattered intensity at the receiver of  $dI_{bs}$ , given by

$$dI_{bs} = \frac{I_{inc}s_v dV}{R^2}. \quad (1)$$

The quantity  $s_v dV$  assumes the role of the backscattering cross section,  $\sigma_{bs}$ , for an assemblage of scatters within elemental volume  $dV$ , where  $s_v$  is the backscattering cross section per cubic meter of water and has units of  $\text{m}^{-1}$ . The total backscattered intensity results from summing all  $dV$ , some of which are away from the acoustic axis, to form the effective scattering volume,  $V$ . For these off-axis contributions, the incident and backscattered intensity are reduced slightly according to the intensity beam pattern  $b(\theta, \phi)$ . The net effect leads to the concept of an effective volume, or reverberation volume [10], based on integration of the two-way intensity pattern  $b^2(\theta, \phi)$ . If we define  $\psi$  as the integral of  $b^2(\theta, \phi)$  over all solid angles, then the effective scattering volume at range  $R$  for a pulse of length  $\tau$  is  $V = \frac{c\tau}{2} R^2 \psi$ , and the total backscattered intensity is

$$I_{bs} = \frac{I_0 r_0^2}{R^4} s_v \frac{c\tau}{2} R^2 \psi, \quad (2)$$

where the incident intensity is referenced back to  $I_0$  via spherical spreading with  $I_{inc} = I_0(r_0/R)^2$  and  $r_0$  is a reference distance set to 1 m. A convenient expression [11] for  $\psi$  which we use in this analysis is

$$\psi = \frac{\pi \phi_W \phi_N}{8 \log_e 2}, \quad (3)$$

where  $\phi_W$  and  $\phi_N$  are the full, one-way  $-3$  dB beamwidths (expressed in radians) for the wide (W) and narrow (N) angles that describe the elliptical HTI transducer beams used in this study. We also use Eq. (3) for the circular Biosonics transducer beams by setting  $\phi_W = \phi_N$ . Values of  $\phi_W$ ,  $\phi_N$ , (in degrees) and  $\psi$  for the two systems during the Kenai measurements are given in Table 1.

The *sonar equation* for volume reverberation is the decibel equivalent of Eq. (2):

$$RL_v = SL - 40 \log_{10} R - 2\alpha R + S_v + 10 \log_{10} \frac{c\tau}{2} R^2 \psi, \quad (4)$$

where  $SL$  is the source level,  $RL_v$  is the reverberation level specifically attributed to volume scattering and is equal to  $10 \log_{10} I_{bs}$ , and the effect of two-way absorption loss is included as  $2\alpha R$ , where  $\alpha$  is the water attenuation coefficient (in dB/m). Given an effective scattering volume  $V$ ,  $10 \log_{10}(s_v V)$  is the equivalent target strength ( $TS$ ) of the scattering volume, which is comparable directly to the  $TS$  of a fish. The *volume scattering strength*,  $S_v$ , is  $10 \log s_v$  (in dB re  $1 \text{ m}^{-1}$ ); this is the key variable pertaining to volume scattering that we shall estimate and report. Note that  $S_v$  can vary with both range and depth. However, with the exception of episodic boat wakes, a range- and depth-independent  $S_v$  is a suitable approximation for the two riverine environments studied here.

Note that the two systems were necessarily configured differently in order to make the kind of measurements demanded by this study. However, with each we ultimately obtained a 100-ping ensemble average of calibrated acoustic intensity for a given time-delay bin; this was equated to range using a nominal sound speed of 1440 m/s. In particular, we worked with ensemble-averaged intensity from the 200-kHz system, whereas we worked with the entire set of 100 pings from the 420-kHz system and computed ensemble averages during postprocessing. The different configurations produce a qualitative difference in the data display, e.g., some small range averaging is already included in the 200-kHz data, but otherwise these differences are of no consequence. The exception is when an occasional fish was detected in some of the measurements, and could not be removed from the 200-kHz ensemble-averaged data. In any case, the primary observable from these measurements is the ensemble-averaged backscattered acoustic intensity versus echo time delay. We report this quantity as the mean reverberation level, or  $RL$  without any subscript, when expressed in dB with reference to  $1 \mu\text{Pa}$ . (The shorthand notation dB re  $1 \mu\text{Pa}$  is hereafter used.) Fluctuations within the 100-ping ensemble were also studied using data from the 420-kHz system.

To estimate  $S_v$  we first computed  $RL$  using data from measurements where the transducer orientation was close to horizontal. At this orientation, the sonar beam ensonifies only a portion of the water column in a given range bin, and backscatter from the surface and bottom boundaries is negligible. We thus assume that the measured  $RL$  is due solely to volume reverberation, and obtain an estimate of  $S_v$  by solving for this quantity in Eq. (4). We remark that  $S_v$  then is also the result of linearly averaging acoustic intensity and then taking the decibel equivalent.

Our estimation procedure is illustrated in the following two figures showing measurements made at 420 kHz with  $\theta_P$  set to  $0^\circ$  (Figure 4) and at 200 kHz with  $\theta_P$  set to  $2^\circ$  (Figure 5). Both measurements were made at approximately noon on 8 June. Figure 4 (top) is an image of the 100 pings versus ping number, or time in seconds, and range from the sonar. The image shows a dramatic increase in  $RL$  at about ping 23 which persists for more than 80 s. This is caused by the bubbly wake of a

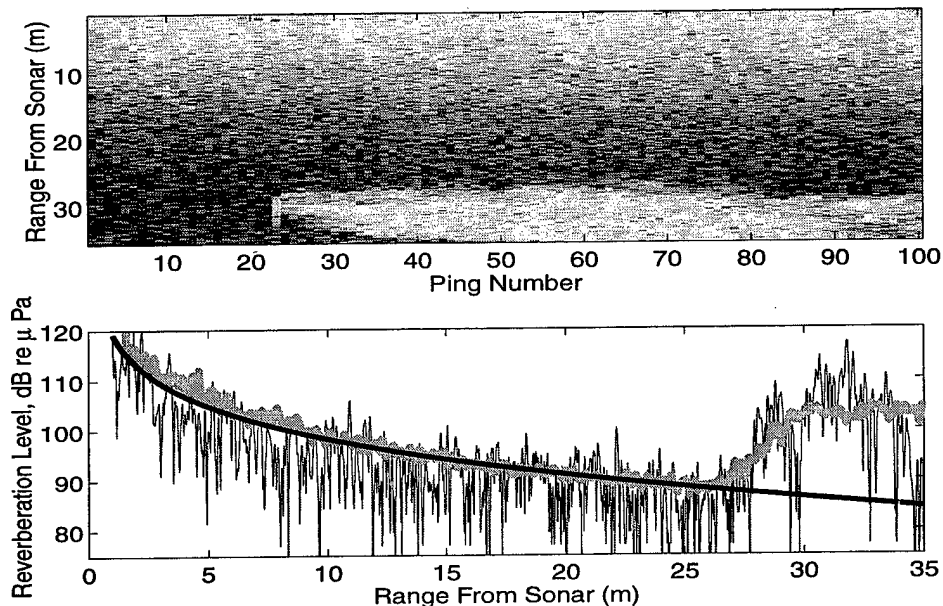


**Figure 4.** Top: Image of 100 pings transmitted at 1-s intervals and a frequency of 420 kHz versus ping number and range from sonar, with lighter shade of gray indicating higher reverberation level. The wake of a passing motor boat can be seen starting at ping 23, and the cross-river dimension of the wake gradually increases from about 2 m to 10 m in 40 s. Bottom: Reverberation level ( $RL$ ) measured during ping number 33 (thin, erratic line), mean  $RL$  based on the 100-ping ensemble average (thick, gray line), and a model for  $RL$  (thick, black line).

passing boat which was also noted in our field observations. The wake broadening caused by turbulent diffusion can be observed, and the cross-river dimension of the wake increases from about 2 m to 10 m in 40 s. Figure 4 (bottom) shows the calibrated reverberation level during ping number 33 (thin, erratic line), plotted along with the mean  $RL$  (thick, gray line) based on the 100-ping ensemble average, and a model for  $RL$  (thick, black line). The model is Eq. (4) evaluated using the source level,  $\alpha = 0.060$  dB/m [8], and  $\psi$  values from Table 1 and with  $S_v$  set to  $-58$  dB, our estimate of  $S_v$  at 420 kHz for this particular run. If we ignore the episodic wake feature, which increases  $S_v$  by about 15 dB, our estimate of  $S_v$  is clearly supported by the data.

Figure 5 shows the equivalent ensemble-averaged  $RL$  versus range measured with the 200-kHz sonar. Here, two runs taken within 4 min of each other are shown by the two gray lines that appear as one, and a third run taken about 10 min later is shown by the thin black line. A model for the mean  $RL$  (thick, black line) again represents an evaluation of the sonar equation using the source level,  $\alpha = 0.013$  dB/m [8], and

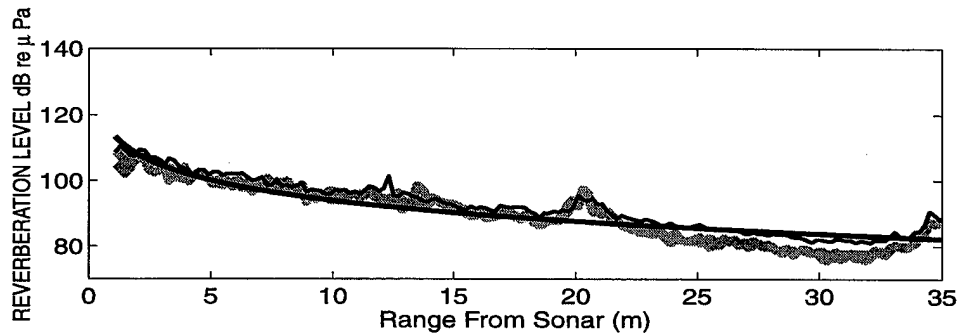


**Figure 5.** Mean  $RL$  at 200 kHz versus range from sonar based on a 100-ping ensemble average (thick gray line) and a model for  $RL$  (thick black line). The thin black line is another measurement of  $RL$  taken approximately 10 min later.

$\psi$  values from Table 1; however, here we have set  $S_v$  to  $-71$  dB, our estimate of  $S_v$  at 200 kHz. The jump in measured  $RL$  near a range of 20 m is likely due to an unknown scattering feature such as a piece of stationary debris; otherwise the estimate of  $S_v$  is well supported by the data. An apparent exception to this agreement begins at a range of 25 m. This range corresponds to the bubble-front of the boat wake seen in Figure 4. There is some evidence from studies of ship wakes that sound absorption within wakes is more severe at 200 kHz than at 420 kHz. However, we have no knowledge of the exact position of the two sonar beams with respect to the wake structure. The 420-kHz beam, for example, could have been ensonifying the more diffuse edge of the wake, while the 200-kHz beam could have been directed toward the more bubble-dense interior of the wake. In any case, a repeat of the 200-kHz measurement approximately 10 min later showed the  $RL$  in the range 20–30 m had returned closer to the values predicted by our model using  $S_v = -71$  dB.

Notwithstanding the differences seen in the response to episodic boat wakes, our estimates of the  $S_v$  at 420 kHz are about 13 dB greater than those at 200 kHz, which implies that Rayleigh scattering is in effect, where the scattered intensity goes as the fourth power of frequency. In the appendix we present a model for Rayleigh scattering from suspended particles associated with the glacial silt load carried in the Kenai River.

Figure 6 shows a sample histogram of  $RL$  at a range of 15 m, computed for each ping of the 100-ping 420-kHz measurement shown in Figure 4. The curve is a probability density function (PDF) and is given by [12]

$$p_s(s) = \frac{e^{-e^{s/k_1}/\lambda + s/k_1}}{k_1 \lambda}, \quad (5)$$

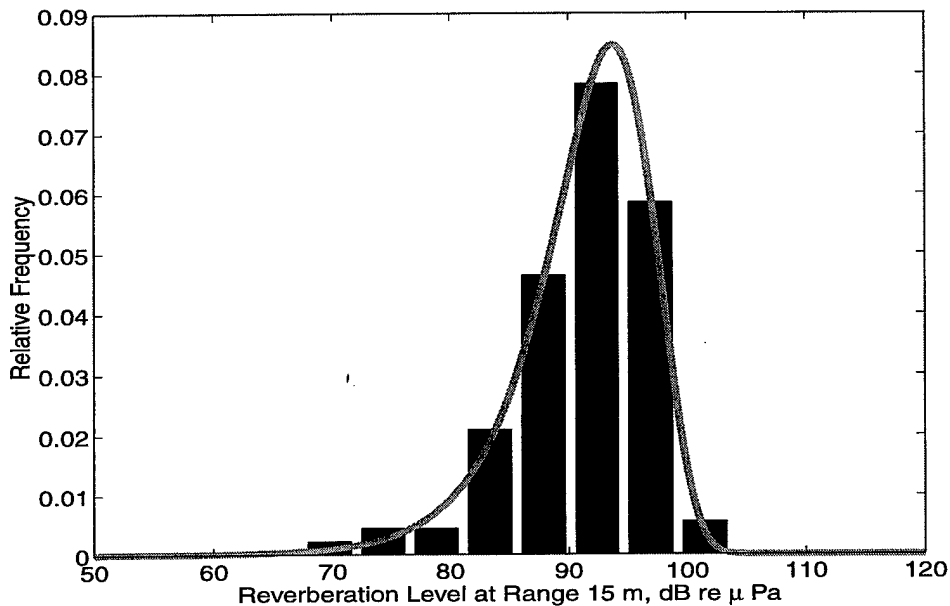


**Figure 6.** Sample histogram of the ping-by-ping 420-kHz reverberation level (in dB) corresponding to a range of 15 m in the data shown in Figure 4. Curve is a model PDF, and significance probability of the  $\chi^2$  statistic is greater than 0.75.

where the random variable  $s$  represents acoustic reverberation level,  $k_1 = 10 \log_{10} e$ , and  $\lambda$  is the mean acoustic reverberation. A chi-square ( $\chi^2$ ) goodness-of-fit test comparing the model PDF with the data shown in Figure 6 results in a significance probability of the  $\chi^2$  statistic being greater than 0.75, suggesting the PDF is a very good model for the observed fluctuations. Since for a given range,  $RL$  and  $S_v$  are related through a constant offset, we can thus say that fluctuations in  $S_v$  for a given range are also distributed according to the PDF given by Eq. (5).

The measurements shown in Figures 4 and 5 each took 100 s to make, and assumptions regarding the stationarity of  $S_v$  in order to compare measurements with the model PDF of Eq. (5) are easily satisfied. Over the 3-hour duration of the experiment, however, we observed a significant variation in our estimates of  $S_v$ . The 30 measurements of  $S_v$  made with the 200-kHz system, for example, were roughly evenly distributed between a high of  $-62$  dB and low of  $-75$  dB. To obtain a measure of the central tendency of  $S_v$ , we choose to average these estimates using  $10 \log_{10}(\langle 10^{S_v/10} \rangle)$ , with the result being  $-67$  dB. This same average performed on the estimates made at 420 kHz yields  $-53$  dB. The difference, about 14 dB, remains close to that predicted by Rayleigh scattering. Finally, we use  $\pm 4$  dB as a measure of the expected spread in  $S_v$  for both the 200-kHz and 420-kHz measurements; this range encompasses 22 of the 30 measurements made at 200 kHz, and 11 of the 15 measurements made at 420 kHz.

## 2.4 Reverberation Due to Bottom Backscattering

Bottom reverberation is the term used to describe acoustic scattering in the direction back toward the transducer from the surface of the riverbed ensonified by the sonar pulse. Some additional notation is now introduced, starting with the sonar equation for backscattering from the riverbed:

$$RL_b = SL - 40 \log R - 2\alpha R + S_b + 10 \log_{10} A - B. \quad (6)$$

In Eq. (6),  $A$  is the effective area of the riverbed contributing to the backscatter,  $RL_b$  is the reverberation level specifically associated with riverbed scattering, and  $B$  is the round-trip beam loss (in dB). Given an effective area,  $A$ , then  $10 \log_{10} A + S_b$  is the equivalent  $TS$  of an area of riverbed with *scattering strength*  $S_b$  (in dB), and it is the key variable pertaining to bottom scattering that we shall estimate and report.

Note that, unlike for  $S_v$ , estimating  $S_b$  using sonar beams that are oriented horizontally is a delicate task. The reverberation caused by scattering from the riverbed reaches the transducer through angles away from that of the transducer's main lobe, and the scattering from the riverbed usually originates at very small grazing angles,  $\theta_G$ . These factors tend to produce a magnified response to very small changes in the scattering geometry, making it more difficult to obtain robust estimates of  $S_b$ . This situation is improved somewhat by pitching the transducer downward, at angle  $\theta_P$ , so that more of the main lobe is pointed toward the riverbed. Figure 7 shows this configuration using a simplified representation of a transducer main lobe. A patch on the riverbed (marked  $A$ ) scatters sound back to the transducer at grazing angle  $\theta_G$ . For a given composition and roughness, the scattering strength,  $S_b$ , of the riverbed is a function only of  $\theta_G$ , which for the geometry shown in Figure 7 is set by

$$\sin \theta_G = H_T \sin(90 + \theta_S)/R. \quad (7)$$

The  $RL_b$  recorded by the transducer, however, depends on the effective launch angle,  $\theta'_L$ , linked to the scattering patch. For geometric considerations, it is convenient to define a vertical launch angle,  $\theta_L$ , with respect to the horizontal, and to define  $\theta'_L$  with respect to the transducer's acoustic axis, which puts  $\theta_L = \theta_G + \theta_S$  and  $\theta'_L = \theta_L - \theta_P$ . The round-trip beam loss is given by  $B = -10 \log_{10} b^2(\theta'_L, 0)$ , where  $b^2(\theta, \phi)$  is the two-way intensity beam pattern as a function of vertical ( $\theta$ ) and azimuthal ( $\phi$ ) angles, and the effective area  $A$  is given by

$$A(\theta'_L) = \frac{c\tau}{2} R \frac{1}{b^2(\theta'_L, 0)} \int_{-\pi}^{\pi} b^2(\theta'_L, \phi) d\phi. \quad (8)$$

To evaluate  $B$ , and the integral in Eq. (8), we construct numerical representations of  $b^2$ , using

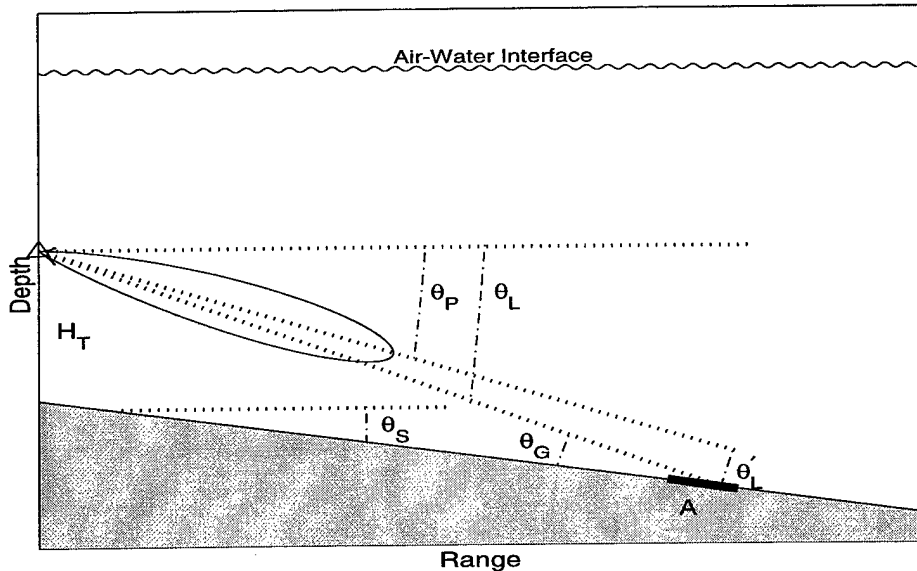


**Figure 7.** The geometry of backscattering from a sloping riverbed. Scattering originates from a patch of riverbed (thick black line labeled A) at the grazing angle  $\theta_G$ . The slope of the riverbed,  $\theta_S$ , the transducer pitch angle,  $\theta_P$ , and the transducer's height above the bottom,  $H_T$ , are the key variables that determine the launch angle,  $\theta_L$ , and the effective launch angle,  $\theta'_L$ , and thereby the reverberation level recorded by the transducer.

$$b^2(\theta, \phi) \approx [b_N(\theta)b_W(\phi)]^2. \quad (9)$$

This approximation is based on the assumption that a one-way intensity pattern defined in both the  $\theta$  and  $\phi$  planes can be specified by multiplying two single-coordinate one-way intensity patterns [13]. The necessary one-way intensity patterns for  $b_N(\theta)$  and  $b_W(\phi)$  were measured by Biosonics and HTI for the transducers used in this study, and the angular resolution in these measurements was increased by interpolation for the purpose of carrying out the integral in Eq. (8).

Figure 8 shows the mean  $RL$  for six sets of measurements at 200 kHz; again, each set represents the ensemble average of 100 pings for which  $\theta_P = 4^\circ$ . Each measurement set was separated by 2 min; two sets were made using a cw transmission length of  $\tau = 0.2$  ms, two sets were made using a cw transmission length of  $\tau = 0.5$  ms, and two sets made using an FM pulse with an effective  $\tau$  of 0.18 ms. The data have been normalized to an equivalent  $\tau$  of 0.2 ms by subtracting 3.98 dB from the measurements made with  $\tau = 0.5$  ms and adding 0.46 dB to the measurements made with an effective  $\tau$  of 0.18 ms. The six measurements agree well following this normalization, which shows that  $RL$  increases or decreases according to  $10 \log_{10} \frac{c\tau}{2}$  (in dB). The dotted-dashed line is modeled  $RL_v$  when using  $S_v = -71$  dB, and the dashed line is modeled  $RL_b$  when using a scattering strength model (in dB) given by

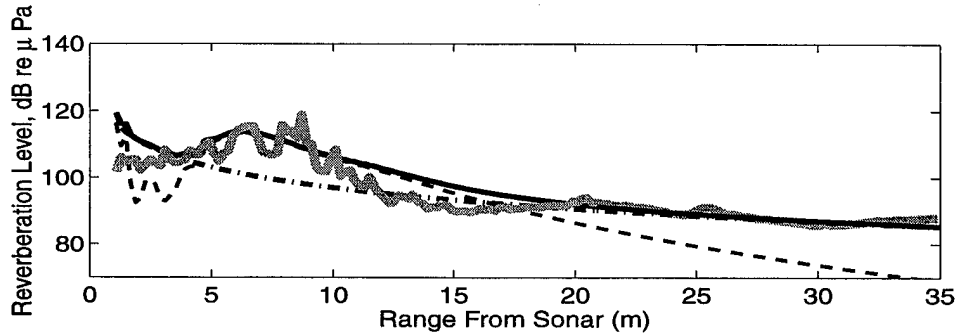


**Figure 8.** Mean  $RL$  measured at 200 kHz versus range from sonar based on 100-ping ensemble average (gray line); model for  $RL_v$  (dotted-dashed line); model for  $RL_b$  (dashed line), and the incoherent sum of  $RL_v$  and  $RL_b$  (solid line).

$$S_b(\theta_G) = 40 \log_{10}(\sin \theta_G) + 2. \quad (10)$$

The solid black line is the incoherent sum of these two components as computed by

$$10 \log_{10}(10^{RL_v/10} + 10^{RL_b/10}). \quad (11)$$

Both the models and the data show that when the transducer is pitched downward to  $\theta_P = 4^\circ$  scattering from the riverbed dominates  $RL$  between ranges of roughly 5 and 10 m, whereas volume scattering tends to dominate outside this region. The models result from evaluating the two sonar equations, Eq. (4) and Eq. (6), using data from Table 1 and the applicable beam-pattern functions  $b_N(\theta)$  and  $b_W(\phi)$ , with  $\theta_P = 4^\circ$  and  $H_T = 0.25$  m being key inputs for the evaluation of  $RL_b$ .

Figure 9 shows the mean  $RL$  for two sets of measurements made at 420 kHz for which  $\theta_P = 8^\circ$ . Each measurement set was also separated by 2 min. One set was made using a cw transmission length of  $\tau = 0.2$  ms, and the other set with  $\tau = 0.4$  ms, which has been normalized to an equivalent  $\tau = 0.2$  ms by subtracting 3 dB. The dotted-dashed line is the modeled  $RL_v$  when using  $S_v = -53$  dB, and the dashed line is the modeled  $RL_b$  when using a scattering strength model (in dB) given by

$$S_b(\theta_G) = 40 \log_{10}(\sin \theta_G) + 7. \quad (12)$$

The solid black line represents the incoherent sum of these two components. As in the example shown in Figure 8,  $\theta_P = 8^\circ$  and  $H_T = 0.48$  m are important inputs for the evaluation of  $RL_b$ . In this case both the models and the data show that when the transducer is pitched downward to  $\theta_P = 8^\circ$  scattering from the riverbed dominates the  $RL$  between ranges of roughly 5 and 20 m, whereas volume scattering tends to dominate outside this region. Note that the data between 5 and 20 m, and also the data shown in Figure 8 between 5 and 10 m, display a slight oscillatory character because

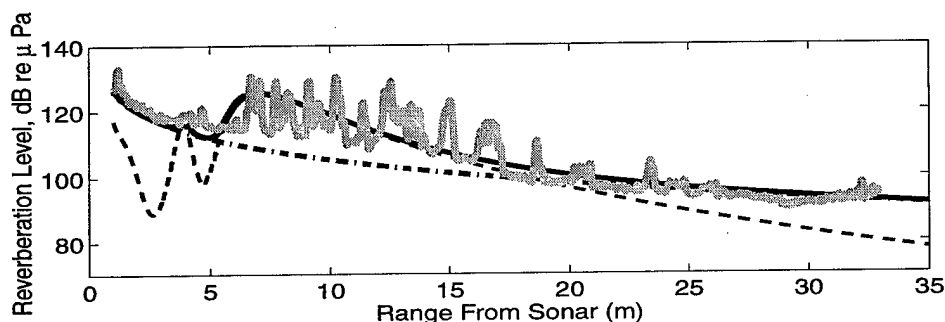


**Figure 9.** Mean  $RL$  measured at 420 kHz versus range from sonar based on 100-ping ensemble average (gray line); model for  $RL_v$  (dotted-dashed line); model for  $RL_b$  (dashed line), and the incoherent sum of  $RL_v$  and  $RL_b$  (solid line).

the mean  $RL$  that originates from the riverbed does not represent a true ensemble, since the same patch of riverbed is ensonified with each ping. Nevertheless, given this deficiency in the measurement, our models for  $RL$  still tend to agree approximately with the data in each case.

The two empirical models for  $S_b$  were derived first by examining estimates of  $S_b$  obtained by inverting Eq. (6), and then mapping the slant range,  $R$ , to the grazing angle  $\theta_G$  to get  $S_b$  versus  $\theta_G$ . We chose to model  $S_b$  using a Bragg scattering law, where  $S_b(\theta_G) \sim 40 \log_{10} \sin(\theta_G)$ . However, only a limited range of grazing angles is involved in scattering from the riverbed. For example, the region of definitive riverbed scattering shown in Figure 9 between about 5 m and 20 m involves grazing angles between only  $2^\circ$  and  $4^\circ$ . It is quite possible that other candidate scattering laws could apply, e.g., Lambert's law, where  $S_b(\theta_G) \sim 20 \log_{10} \sin(\theta_G)$ . When comparing the resultant total  $RL$  with the measured  $RL$ , though, the  $40 \log_{10} \sin(\theta_G)$  dependence produced the most acceptable result. Were Bragg scattering to be the true modality for acoustic backscattering from the riverbed, then this scattering would originate from roughness at very small scales corresponding to the Bragg wavelength, which is half the acoustic wavelength for small  $\theta_G$ , i.e., 1.7 mm at 420 kHz and 3.6 mm at 200 kHz. However, other, corner-reflecting features such as larger pebbles and rocks could very well be contributing to the scattering in a major way, and it is unlikely that Bragg scattering alone is the source of riverbed scattering.

Finally, radar observations [13] of backscattering from gravel roads at the equivalent radar wavelength in air also show the scattering to increase with frequency as we observe.

### 3 MEASUREMENTS IN THE WOOD RIVER

#### 3.1 Site Description and Geometry

The Wood River measurements were made on 4 and 5 July 1999 at a site on the right bank about 18 miles upstream from the river's entry into Nushagak Bay (Fig. 10). This site represents an interesting contrast to the one on the Kenai River. First, the Wood River originates from an outlet of Lake Aleknagik. The water is remarkably clear and free of turbidity, and for nearly 50 years ADF&G has been using this site, and a similar one on the left bank, to visually estimate escapements of migrating sockeye salmon (*Oncorhynchus nerka*). Visual counts of salmon are made from atop 20-ft counting towers placed near the banks at distances to the water exceeding 30 ft. Second, the overall geometric scale in terms of sonar ranges and depths is smaller at the Wood River site. Currents in the Wood River are considerably faster, typically 1–1.5 m/s, and the smaller sockeye salmon tend to swim in tight bands 1–2 m wide within 1–5 m of the river bank [14] to take advantage of more turbulent flow conditions and thereby conserve energy. Thus, our acoustic measurements at this site were limited to ranges  $\leq 6$  m (with a few measurements made beyond this range) and to depths less than about 1 m.

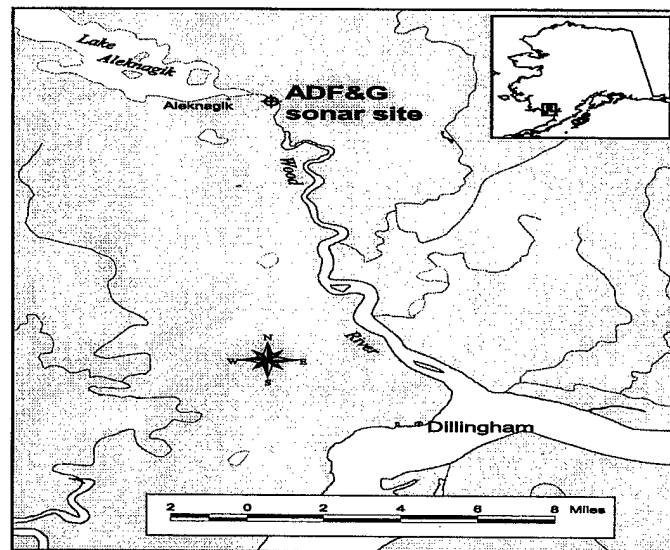
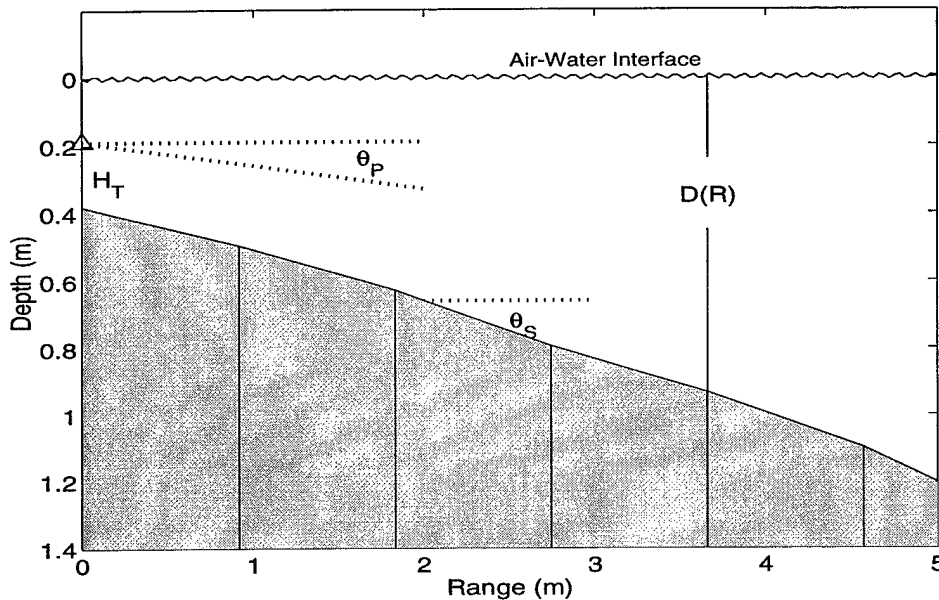


Figure 10. Map of the Wood River showing the location of the sonar test site.

Figure 11 shows the position of the HTI transducer, with  $H_T = 0.19$  m, and the bottom contour out to about 5 m in range, which was the limit that could be measured directly with a probe. The Biosonics location was similar, with  $H_T = 0.20$  m. The bottom slope varied slowly with range, with an average slope,  $\theta_S$ , of  $8^\circ$ . No CTD measurements were made at this site as the water was considered both well mixed and free of salinity. (There is a small tidal effect that influences the river current, which we discuss later.) The water temperature was  $8^\circ\text{C}$ , setting the sound speed,  $c$ , equal to  $1438.5$  m/s, and we again use  $\alpha = 0.013$  dB/m at 200 kHz and  $\alpha = 0.060$  dB/m at 420 kHz.



**Figure 11.** Experimental geometry for the acoustic reverberation measurements made in the Wood River and key geometric variables. View represents a portion of the river cross section at its right bank extending out about 5 m corresponding to the location of the HTI system. The transducer's position is shown by the large triangle at range = 0 m. The bottom contour has been constructed from depth readings made with a probe.

### 3.2 Acoustic Measurements

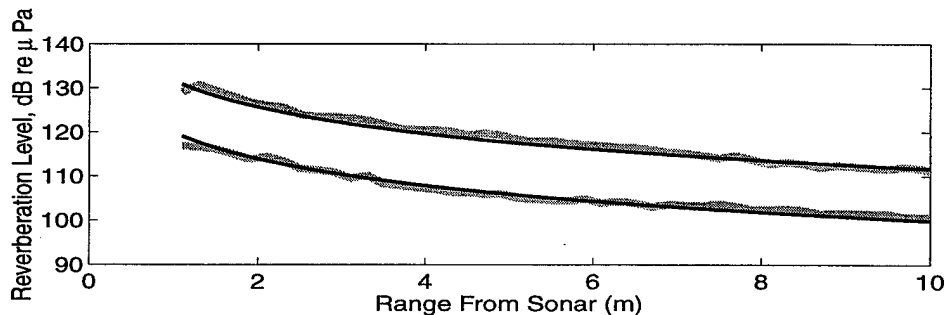
For the 420-kHz system the optimum transducer pitch angle for counting fish,  $\theta_{PF}$ , was found to be  $8^\circ$ , and measurements were made at this angle and at  $6^\circ$ ,  $10^\circ$ ,  $0^\circ$ , and  $-2^\circ$ . For the 200-kHz system  $\theta_{PF}$  was found to be  $7^\circ$ , and measurements were made at this angle and at  $5^\circ$ ,  $9^\circ$ ,  $0^\circ$ , and  $-2^\circ$ . (The transducer pitch angles reported here are to the nearest degree.) As at the Kenai River site, the optimum

transducer pitch angle also comes close to the average slope of the riverbed. Key sonar system parameters used during the Wood River measurement phase are summarized in Table 2.

**Table 2.** Sonar system parameters used for acoustic measurements in the Wood River.

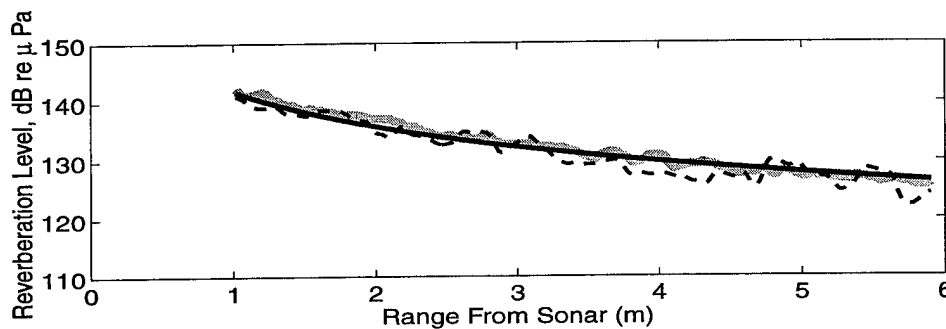
System	Frequency (kHz)	Source Level (dB)	$\phi_W$ (deg)	$\phi_N$ (deg)	$10 \log_{10} \psi$ (dB)
Biosonics (circ.)	420	212.4	4.7	4.7	-24.2
Biosonics (ellip.)	420	217.5	7.1	2.6	-25.0
HTI (circ.)	200	216.3	6	6	-21.3
HTI (ellip.)	200	213.8	6	10	-20.2

Figure 12 shows the results of two ensemble-averaged  $RL$  measurements (gray lines) versus range made with the 200-kHz sonar, for which  $\theta_P$  was  $0^\circ$ . The upper curves represent measurements made on 4 July at approximately 1700, and the lower curves represent measurements made on 5 July at approximately 1200. The models for mean  $RL$  (black lines) result from evaluating the sonar equation using the data shown in Table 2 for the 200-kHz circular transducer; the upper curve is based on  $S_v = -55$  dB, and lower curve on  $S_v = -66$  dB.



**Figure 12.** Mean  $RL$  measured at 200 kHz versus range based on a 100-ping ensemble average (gray lines), and a model for  $RL$  (black lines). Upper measurements were made on 4 July at approximately 1700, and the lower measurements were made on 5 July at approximately 1200.

Figure 13 shows the results of two ensemble-averaged  $RL$  measurements versus range made with the 420-kHz sonar for  $\theta_P = 0^\circ$  (gray line) and  $\theta_P = 8^\circ$  (dashed line), which is discussed further below. The measurements were made on 4 July at approximately 1700. The model for the mean  $RL$  (thick, black line) is the result of evaluating the sonar equation using the data shown in Table 2 for the 420-kHz elliptical transducer, based on  $S_v = -42$  dB.



**Figure 13.** Mean  $RL$  measured at 420 kHz versus range based on a 100-ping ensemble average for  $\theta_P = 0^\circ$  (thick, gray line) and  $\theta_P = 8^\circ$  (dashed line), and a model for  $RL$  (thick, black line).

The 4 July estimates of  $S_v$  at 200 kHz and 420 kHz differ by about 13 dB, which again strongly suggests that Rayleigh scattering is in effect. The source of this scattering in the clear and fast moving water of the Wood River is most certainly small bubbles with radii  $\leq 10 \mu\text{m}$  (see appendix). There is a difference of 11 dB between the 200-kHz measurements made on 4 July and 5 July, which we believe is linked to the tidal cycle that determines the river currents. Unfortunately, scheduled current measurements had to be cut back owing to instrument difficulties, and no current measurements were made close to the time of the acoustic measurements. However, the 4 July acoustic measurements were made about an hour after low tide as measured at Clark's Point near the river's entry into Nushagak Bay, while the 5 July measurements were made 2–3 hours after a 20-ft high tide at Clark's Point. The relation between the tidal elevation at Clark's Point and river currents is such that the river current at the measurement site would have been swifter during the 4 July measurements [15]. The swifter current would provide more opportunity for bubble creation, which would increase the acoustic scattering as was observed.

Figure 14 is a sample histogram of the  $RL$  at a range of 5 m, computed for each ping of the 100-ping 420-kHz measurement shown in Figure 13, compared with the PDF given by Eq. (5) (curve). The probability of the  $\chi^2$  statistic in this case is greater than 0.5, suggesting that the PDF model is also a good one for the  $RL$  (and  $S_v$ ) observed in the Wood River, provided stationarity assumptions are satisfied.

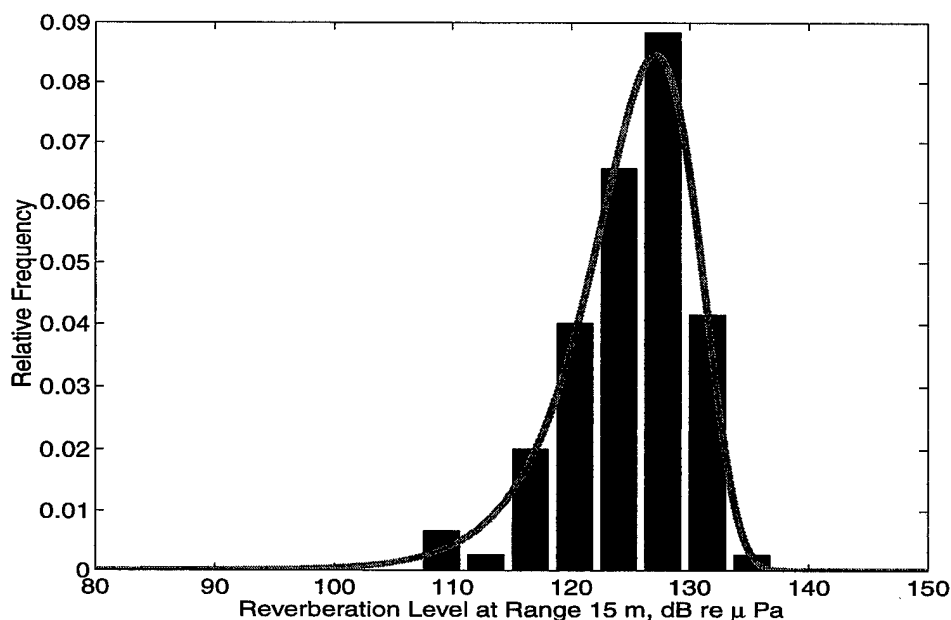


**Figure 14.** Sample histogram of the ping-by-ping 420-kHz reverberation level (in dB) corresponding to the data shown at a range of 5 m in Figure 13. Curve is a model PDF, and the  $\chi^2$  probability statistic is greater than 0.5.

For both the 200-kHz and 420-kHz measurements made on 4 July between 1630 and 1730, the variation in  $S_v$  ( $\pm 2$  dB) was smaller than the variation of  $\pm 4$  dB for the Kenai River measurements. But the large change in  $S_v$  between the measurements made on 4 July and 5 July at 200 kHz shows the degree to which tidal-induced changes in river currents, and therefore bubble production, can affect  $S_v$ . For a measure of the expected spread in  $S_v$  for the Wood River site, we thus take the entire range, i.e.,  $-55$  dB to  $-66$  dB for 200 kHz and  $-42$  dB to  $-53$  dB at 420 kHz. Note that we infer the lower limit ( $-53$  dB) at 420 kHz from that expected for Rayleigh scattering, given a measured  $S_v$  of  $-66$  dB at 200 kHz.

Finally, the July measurements at Wood River fell well within the peak migratory period of sockeye salmon and, unlike during the Kenai measurements, it was difficult to find time segments during which there were significant gaps in fish passage. Although there were attempts to divert fish away from the acoustic beams, most measurements made at pitch angles corresponding to  $\theta_{PF}$  and greater showed evidence of scattering from fish. Thus we were unable to obtain reliable estimates of scattering from the riverbed without significant contamination by scattering from fish. A reasonable starting model, however, would be the model equations for  $S_b$  at 200 and 420 kHz obtained for the Kenai measurements. In some cases, though, pings showing evidence of fish scattering could be removed from the 100-ping ensemble collected by the Biosonics system before computing the ensemble average. An example of such a correction is shown by the dashed line in Figure 13 representing the  $RL$

measured when  $\theta_P$  was  $8^\circ$ , the optimum pitch angle for fish detection. The reasonable agreement with the modeled  $RL$  based on volume scattering alone suggests that, as for the Kenai River, background reverberation at the Wood River site is set by  $S_v$  for sonar fish-counting geometries.

## 4 SUMMARY AND CONCLUSIONS

Environmental acoustic measurements were made in two distinct Alaskan riverine environments during the summer of 1999: in the slower-flowing and more turbid Kenai River, and in the faster-flowing and clear Wood River. The goal of these measurements was to understand, and model, the sources and magnitude of background acoustic reverberation, defined as the average acoustic intensity versus time (range) in the absence of any contribution by scattering from fish. The measurements were made using a 200-kHz and a 420-kHz sonar system, in conditions and geometries that simulated the optimum configuration for riverine-sonar fish counting. In addition, the configurations were altered by changing the transducer pitch angle,  $\theta_P$ , in order to isolate the contributions of scattering from the water volume and scattering from the riverbed to the total background reverberation.

The measurements produced estimates of the calibrated, ensemble-averaged background reverberation level,  $RL$  (in dB re  $\mu\text{Pa}$ ), based on a 100-ping ensemble and estimates of the variance of this quantity. We modeled  $RL$  as the incoherent sum of two components. One,  $RL_v$ , is volume scattering from entrained bubbles and silt particles, for which the key determinate variable is volume scattering strength  $S_v$  (in dB). The other,  $RL_b$ , is scattering from the riverbed, for which the key determinate variable is the riverbed scattering strength  $S_b$  (in dB). Note that a third contribution is scattering from the water surface. However, this contribution is negligible in comparison to, and cannot be distinguished from, volume scattering from the region near the surface.

Our study shows that volume scattering, and thus  $S_v$ , is the more important of the two primary scattering contributions. For example, when the sonar beams were optimally aimed for fish counting—typically a few degrees below horizontal at a pitch angle,  $\theta_P$ , close to the average slope of the riverbed,  $\theta_S$ , the measured  $RL$  was well modeled by an equation for  $RL_v$  in which the inputs were the particular sonar parameters used during the measurements of  $RL$  and  $S_v$ . For the Kenai River site, we estimated  $S_v$  to be  $-53 \text{ dB} \pm 4 \text{ dB}$  at 420 kHz and  $-67 \text{ dB} \pm 4 \text{ dB}$  at 200 kHz. The difference,  $40 \log_{10} 420/200$ , is that predicted by Rayleigh scattering. For the Wood River site, we estimated that  $S_v$  ranged from  $-55 \text{ dB}$  to  $-66 \text{ dB}$  at 200 kHz and from  $-42 \text{ dB}$  to  $-53 \text{ dB}$  at 420 kHz. This larger range was associated with tidally influenced river currents, which would modulate the bubble density by producing more bubbles when the water was swifter.

We also modeled fluctuations in  $RL$ , and demonstrated that under stationary conditions fluctuations at a fixed range are well described by a probability density function (PDF) given by Eq. (5). This also means that fluctuations in  $S_v$  at a fixed range are described by the same PDF when stationarity applies. However, as noted

by the reported range in estimates of  $S_v$ , stationarity can typically be assumed to apply for only short periods. In future work we will investigate an alternative PDF that would apply to a slowly varying  $S_v$ , as discussed by Dahl and Plant [12].

A model for  $S_v$  due to scattering from glacial silt particles suspended in the water, and thus applicable to the Kenai River, is presented in the appendix. Although the model estimates of  $S_v$  agreed quite well with the  $S_v$  measured at 200 kHz and 420 kHz, we caution that a possible added contribution due to scattering from bubbles is difficult to distinguish without additional analysis. The model should motivate, however, further study on the relationship between  $S_v$  and turbidity, as measured in nephelometric turbidity units (NTU), and it may be particularly useful for acoustical-limnological studies in Alaskan lakes containing glacial meltwater.

Our study quantifies how fish detection using horizontal-looking sonars in rivers is reverberation limited and not noise limited. This agrees with Trevorrow's study [16] of the background reverberation in horizontal-looking sonars in Canada's Fraser River. Increasing the source level ( $SL$ ), then, increases the amplitude of not only the fish echoes but also the background  $RL$ , and thus the ratio of fish-to-background amplitude remains the same.

Knowing  $S_v$ , and proceeding with the idea that volume scattering alone establishes the background reverberation level, then makes a number of important estimates possible. One is the minimum fish target strength,  $TS_{\min}$ , that can be reliably detected. Assuming, for example, that  $TS_{\min}$  must be at least 10 dB greater than the equivalent target strength of the volume of water ensonified,  $TS_{\text{vol}}$ , then the simple relation follows that  $TS_{\min} \geq TS_{\text{vol}} + 10$  dB, where

$$TS_{\text{vol}} = 10 \log_{10} \left( \frac{c\tau}{2} R^2 \psi \right) + S_v. \quad (13)$$

Equation (13) can be used to evaluate the effect of different combinations of pulse length,  $\tau$ , sonar beams as parameterized by  $\psi$ , and ranges,  $R$ , on fish-detection goals and algorithms. More realism can be introduced in Eq. (13) by applying statistical models for both  $S_v$  and fish target strength. In terms of  $S_v$  the PDFs discussed here and in Ref. 12 will be useful. Regarding fish target strength, Dahl and Mathisen [17] have shown that measurements of the target strength of salmon at side aspect, under controlled conditions, are also distributed according to the PDF given by Eq. (5), and an aspect dependence in the mean  $TS$  is also discussed. More recent studies by Burwen and Fleischman [18] and Kubečka [19] address how fish aspect and orientation in the riverine environment influence  $TS$  and the PDF for fish target strength.

Another important estimate that we can make based on knowledge of the background reverberation level is the rms error in angular location estimates,  $\theta_{\text{rms}}$ , made with split-beam sonars for the purpose of fish tracking. This error in radians is given

by [20]

$$\theta_{\text{rms}} = \frac{1}{2\pi\sqrt{\text{SNR}d/\lambda}}, \quad (14)$$

where  $d$  is the effective horizontal separation between the transducer half beams in a split-beam system,  $\lambda$  here stands for acoustic wavelength, and SNR is the full beam signal-to-noise ratio. For this case, the applicable SNR can be estimated by

$$\text{SNR} = 10^{(TS_{\text{fish}} - TS_{\text{vol}})/10}, \quad (15)$$

where  $TS_{\text{fish}}$  is the nominal target strength of a fish at side aspect, and  $TS_{\text{vol}}$  is given by Eq. (13).

## REFERENCES

1. Royce, W. F., "Managing Alaska's salmon fisheries for a prosperous future," *Fisheries*, **14**(2), 8-13, 1989.
2. Beamish, R. J., and D. R. Bouillon, "Pacific salmon production trends in relation to climate," *Can. J. Fish. Aquat. Sci.*, **50**, 1002-1016, 1993.
3. Adkison, M. D., R. M. Peterman, M. F. Lapointe, D. M. Gillis, and J. Korman, "Alternate models of climate effects on sockeye salmon, *Oncorhynchus nerke*, productivity in Bristol Bay, Alaska, and Fraser River, British Columbia," *Fisheries Oceanography*, **5**(3/4), 137-152, 1996.
4. Davis, A. S., "Salmon counting by acoustic means," *Informational Leaflet 113*, Alaska Department of Fish and Game, Division of Commercial Fisheries, Juneau, Alaska, 1968.
5. Gaudet, D., "Enumeration of migratory salmon populations using fixed-location sonar counters," *Rapp. P.-V. Reun., Cons. Int. Explor. Mer.*, **189**, 197-209, 1990.
6. Burwen, D. L., D. Bosch, and S. J. Fleishman, "Evaluation of hydroacoustic assessment techniques for chinook salmon on the Kenai River, 1995," Fishery Data Series No. 98-3, Alaska Department of Fish and Game, Anchorage, 1998.
7. Bosch, D., and D. L. Burwen, "Estimates of chinook salmon abundance in the Kenai River using split-beam sonar, 1997," Fishery Data Series No. 99-3, Alaska Department of Fish and Game, Anchorage, 1999.
8. Dahl, P. H., "Underwater Ultrasound," in *Encyclopedia of Electrical and Electronics Engineering*, J. G. Webster, Ed., John Wiley & Sons, New York, 1999, pp. 10-27.
9. Dahl, P. H., and O. A. Mathisen, "Some experiments and considerations for development of Doppler-based riverine sonars," *IEEE J. Oceanic Eng.*, **OE-9**, 214-217, 1984.
10. R. Urick, *Principles of Underwater Sound*, McGraw-Hill, 1983.
11. Probert-Jones, J. R., "The radar equation in meteorology," *Quar. J. Roy. Meteor. Soc.*, **88**, 485-495, 1962.
12. Dahl, P. H., and W. A. Plant, "The variability of high-frequency acoustic backscatter from the region near the sea surface," *J. Acoust. Soc. Am.* **101**, 2596-2602, 1997.

13. Skolnik, M., *Introduction to Radar Systems*, McGraw-Hill, 1980.
14. Mathisen, O.A., "Photographic enumeration of red salmon escapement," in *Studies of Alaska Red Salmon*, University of Washington Press, 1962.
15. Mathisen, O.A., personal communication, February 2000.
16. Trevorrow, M. E., "Detection of migrating salmon in the Fraser River using 100-kHz sidescan sonars," *Can. J. Fish. Aquat. Sci.*, **54**, 1619–1629, 1997.
17. Dahl, P. H., and O. A. Mathisen, "Measurement of fish target strength and associated directivity at high frequencies," *J. Acoust. Soc. Am.*, **73**, 1205–1211, 1983.
18. Burwen, D., and S. J. Fleischman, "Evaluation of side-aspect target strength and pulse width as potential hydroacoustic discriminators of fish species in rivers," *Can. J. Fish. Aquat. Sci.*, **55**, 2492–2502, 1998.
19. Kubečka, J., "Simple model on the relationship between fish acoustical target strength and aspect for high-frequency sonar in shallow waters," *J. Appl. Ichthyol.*, **10**, 75–81, 1994.
20. Ehrenberg, J. E., and T. C. Torkelson, "Application of dual-beam and split-beam target tracking in fisheries acoustics," *Rapp. P.-V. Reun., Cons. Int. Explor. Mer.*, **53**, 329–334, 1996.
21. Medwin, H., and C. S. Clay, *Fundamentals of Acoustical Oceanography*, Academic Press, 1998.
22. May, A. E., and R.W. Burling "On sound scattering and attenuation in suspensions, with marine applications," *J. Acoust. Soc. Am.*, **72**, 950–959, 1982.
23. Asher, W. E., L. M. Karle, and B. J. Higgins, "On the difference between bubble-mediated air–water transfer in freshwater and seawater," *J. Mar. Res.*, **55**, 813–845, 1997.
24. These data were kindly made available by the Alaska Department of Fish and Game, Sport Fish Division, Soldotna, Alaska, through the assistance of Mr. Daniel Bosch.
25. Edmundson, J. A., and J. P. Koenings, "The effects of glacial silt on primary production, through altered light regimes and phosphorus levels, in Alaska lakes," *Proceedings, Resolving Alaska's Water Resource Conflicts*, Report IWR-108, University of Alaska-Fairbanks, 1985, pp. 3–19.

26. Koenings, J. P., and J. A. Edmundson, "Secchi disk and photometer estimates of light regimes in Alaskan lakes: Effects of yellow color and turbidity," *Limnol. Oceanogr.*, **36**, 91-105, 1991.
27. Edmundson, J. A. Equation (A4) was provided by J. A. Edmundson of the Alaska Department of Fish and Game, personal communication, January 2000.

## APPENDIX

**Comparative Measures of Scattering from Bubbles and Glacial Silt  
Particles and a Model Relating Turbidity Measures to Volume Scattering  
from Glacial Silt Particles**

Two primary sources of volume backscattering were observed in this study. One is small bubbles whose radii are less than about  $10 \mu\text{m}$ , as we discuss further below. Bubble scattering would be in effect in both the Kenai and Wood rivers, but we would expect the bubble concentration to be greater in the faster flowing, and more turbulent, Wood River. The other source is particles associated with glacial silt whose radii are also about  $10 \mu\text{m}$ . This source would apply only to the Kenai River, which carries a load of glacial silt, as the water at the Wood River site is very clear with negligible turbidity.

Figure A1 shows the backscattering cross section,  $\sigma_{bs}$  (expressed in dB), for a single bubble or particle of glacial silt versus bubble or particle radius,  $a$ , computed using equations discussed in standard texts, e.g., Ref. 21. For the bubble we use

$$\sigma_{bs} = \frac{a^2}{[(f_R/f)^2 - 1]^2 + \delta^2}, \quad (\text{A1})$$

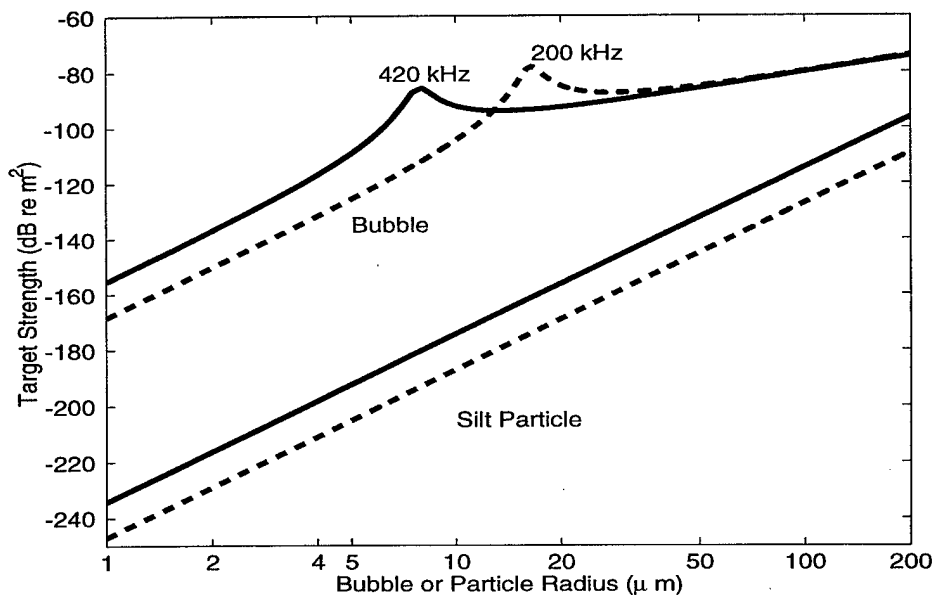


**Figure A1.** Backscattering cross section,  $\sigma_{bs}$  (expressed in dB), for a single bubble or particle of glacial silt versus bubble or particle radius,  $a$ , for acoustic frequencies of 420 kHz (solid line) and 200 kHz (dashed line).

where  $f$  is acoustic frequency,  $\delta$  is the total damping coefficient (approximated by  $\delta = 2.55 \times 10^{-3} f^{1/3}$ ), and all values are expressed in MKS units. Scattering is maximal at a frequency equal to the resonant frequency,  $f_R$ , for a bubble of radius  $a_R$ . Since we are dealing with very shallow depths,  $f_R$  and  $a_R$  are related by  $a_R \approx 3.25/f_R$  (MKS). The peaks shown in the figure are associated with resonant scattering and correspond to a radius,  $a$ , of about  $7.7 \mu\text{m}$  for 420 kHz and  $16 \mu\text{m}$  for 200 kHz.

For a silt particle we use

$$\sigma_{bs} = (ka)^4 \left[ \frac{e-1}{3e} + \frac{g-1}{2g+1} \right]^2 a^2, \quad (\text{A2})$$

where  $k$  is the acoustic wavenumber (1829 radians/m at 420 kHz and 871 at 200 kHz),  $e$  is the ratio of the elasticity of the particle to that of the water, and  $g$  is the ratio of the density of the particle to that of the water. For  $e$  and  $g$  we require the density and compressional wave speed of a silt particle, values that depend on the specific mineral properties and degree of homogeneity of silt. A reasonable starting point is to assume that the silt material properties are like those of sand and quartz, with a density and compressional wave speed in the neighborhood of  $2650 \text{ kg/m}^3$  and  $5100 \text{ m/s}$ , respectively [22]. These values set  $e$  equal to 32.78 and  $g$  equal to 2.65.

Our data are very clear insofar as we consistently observed a difference of approximately 13 dB in the estimates of  $S_v$  derived from measurements made at 200 kHz and 420 kHz. This implies that Rayleigh scattering, in which the scattered intensity goes as the fourth power of frequency, is in effect. As shown by the upper two parallel lines separated by 12.9 dB in Figure A1, Rayleigh scattering applies for bubbles whose radii are less than about  $7 \mu\text{m}$ . Rayleigh scattering from silt applies for particle radii up to at least  $200 \mu\text{m}$  (at which point we end our calculation). Another important consequence of Rayleigh scattering is that the scattered intensity goes as the sixth power of the radius,  $a$ . The  $\sigma_{bs}$  for a  $20\text{-}\mu\text{m}$  silt particle, for example, is 18 dB greater than that for a  $10\text{-}\mu\text{m}$  silt particle.

Recall that our observable, however, is not  $\sigma_{bs}$  but rather the backscattering cross section per unit volume,  $s_v$  (or its decibel equivalent  $S_v$ ), which is defined by the integral

$$s_v = \int_a \sigma_{bs}(a) N(a) da. \quad (\text{A3})$$

The distribution function  $N(a)$  gives the number of particles, or bubbles, per cubic meter with radii between  $a$  and  $a + da$ , and thus is analogous to a probability density function (PDF) for bubble or particle radius.

Bubbles within a wide size range will, in fact, be produced by the breaking of the water surface existing in areas with fast currents or areas with flow obstructions caused by large rocks. Larger bubbles quickly rise to the surface, but smaller ones are

easily advected a few meters below the surface by turbulent diffusion. The persistence time of smaller bubbles (radii  $< 10 \mu\text{m}$ ) is lengthened in the cold, highly-oxygenated riverine water, which invariably contains surfactants associated with biological activity [23].

Thus we postulate that bubbles with radii  $< 10 \mu\text{m}$  are the only source of the volume scattering observed in the shallower, faster flowing, and more turbulent Wood River. We do not have sufficient information to characterize the size distribution of these bubbles further, other than the one linked to Rayleigh scattering. Bubbles are also likely to be a source of volume scattering in the Kenai River. We expect bubble concentration in the Kenai River to be less than that found in the Wood River, however, since the current is slower in the Kenai. The exception is wakes from boat traffic in the Kenai, which we have shown to produce an enormous increase in  $S_v$  associated with bubble scattering.

The significant load of glacial silt carried in the Kenai River and the resulting turbidity, however, mean that scattering from suspended particles also contributes to the volume backscatter. It is not possible to determine the exact relative contribution of each source, bubbles and silt particulates, to acoustic volume scattering because we do not have the requisite ancillary data on *in situ* bubble and silt particulate size distribution and concentration. We can, however, make a first-cut evaluation. For this, we shall use some empirical relations for three limnology variables that have been measured by scientists from ADF&G in Alaskan lake and riverine systems that are influenced by glacial meltwater.

The first variable is the depth,  $SD$  (in meters), to which a secchi disk can be seen (the secchi transparency depth), which is a measure of water transparency. ADF&G biologists recorded  $SD$  about 3 times daily on the Kenai River at a site near our experimental area. From these recordings [24] we estimate that the  $SD$  was approximately 0.6 m at the time of our volume scattering measurements.

The second variable is turbidity expressed in nephelometric turbidity units, or NTU. We will see that NTU is a key variable for examining acoustic volume scattering from glacial silt, because of its strong correlation to both particle concentration and mean particle radius [25]. Turbidity levels are inversely proportional to the light compensation depth as determined by a secchi disk reading [25], and an empirical relation predicting  $SD$  as a function of turbidity expressed in NTU has been demonstrated by Koenings and Edmundson [26] using data from several Alaskan lakes influenced by glacier meltwater. Edmundson [27] kindly re-examined data from 15 Alaskan lakes with turbidities that encompass the range of measurements in the Kenai River and derived the following relation enabling us to use  $SD$  as a *model predictor* of NTU:

$$\log_{10}(\text{NTU}) = 0.952 - 1.093 \log_{10}(\text{SD}) \quad (\text{A4})$$

with squared correlation coefficient  $r^2 = 0.89$ . Using Eq. (A4) and  $SD = 0.6$  m gives an estimate of  $NTU = 16$ .

The third variable is mean particle size,  $PS$  (or diameter). Edmundson and Koenigs [25] also show that  $PS$  is also strongly correlated with  $NTU$ . We have re-digitized the data presented in Figure 1A of Ref. 25 in order use  $NTU$  as a model predictor of  $PS$  in microns. The result is

$$\log_{10}(PS) = -0.355 \log_{10}(NTU) + 1.704 , \quad (A5)$$

with  $r^2 = 0.75$ . Using Eq. (A5) with  $NTU = 16$  puts  $PS$  equal to about  $19 \mu\text{m}$ , for a mean particle radius,  $a$ , between  $9$  and  $10 \mu\text{m}$ .

To proceed further, we require a description of  $N(a)$ . The primary author (Dahl) has examined an unpublished set of histograms of particle sizes in samples of glacial meltwater taken in the mid-1980s by scientists from ADF&G. A Rayleigh probability density function (PDF) appears to be a reasonable model for these histograms. The Rayleigh PDF as a function of particle radius,  $a$ , is

$$p_a(a) = \frac{a}{\alpha_a^2} e^{-a^2/2\alpha_a^2}. \quad (A6)$$

The PDF is governed by  $\alpha_a$ , which is related to the expected value of particle radius,  $E(a)$ , by  $E(a) = \alpha_a \sqrt{\frac{\pi}{2}}$ . By hypothesis, we equate  $E(a)$  to mean particle radius, or  $PS/2$ , as determined by Eq. (A5). The particle size distribution,  $N(a)$ , used in Eq. (A3) is  $PN \times p_a(a)$ , where  $PN$  is the total number of particles per cubic meter. We can now estimate  $PN$  using Eq. (A3), along with our nominal observed values of  $S_v$  for the Kenai River which are  $-67$  dB at  $200$  kHz and  $-53$  dB at  $420$  kHz. These values for  $S_v$ , combined with the above assumptions, give a  $PN$  on the order of  $10^{11}$  silt particles per cubic meter.

This is plausible value for  $PN$ . However, there are still many issues to resolve. One is the degree of flocculence of the suspended silt particulates, i.e., the degree to which the particulates have coalesced. Another is the relative contribution of bubbles to the total volume scattering.

Thus, the main purpose of this analysis is to serve as a guide and to motivate further study of the relationship between  $S_v$  and turbidity as measured in units of  $NTU$ . For example, a longer time series of simultaneous measurement of  $S_v$ ,  $NTU$ , and  $SD$  at the minimum, and if resources permit, histograms of particle size distribution, would help clarify several issues.

# REPORT DOCUMENTATION PAGE

Form Approved  
OPM No. 0704-0188

Public reporting burden for this collection of information is estimated to average 1 hour per response, including the time for reviewing instructions, searching existing data sources, gathering and maintaining the data needed, and reviewing the collection of information. Send comments regarding this burden estimate or any other aspect of this collection of information, including suggestions for reducing this burden, to Washington Headquarters Services, Directorate for Information Operations and Reports, 1215 Jefferson Davis Highway, Suite 1204, Arlington, VA 22202-4302, and to the Office of Information and Regulatory Affairs, Office of Management and Budget, Washington, DC 20503.

1. AGENCY USE ONLY (Leave blank)		2. REPORT DATE August 2000	3. REPORT TYPE AND DATES COVERED Technical	
4. TITLE AND SUBTITLE The Environmental Acoustics of Two Alaskan Rivers and its Relation to Salmon Counting Sonars			5. FUNDING NUMBERS ADF&G Contract IHP-98-003	
6. AUTHOR(S) Peter H. Dahl, Harold J. Geiger, Deborah A. Hart, James J. Dawson, Sam V. Johnston, & Donald Degan				
7. PERFORMING ORGANIZATION NAME(S) AND ADDRESS(ES) Applied Physics Laboratory University of Washington 1013 NE 40th Street Seattle, WA 98105-6698			8. PERFORMING ORGANIZATION REPORT NUMBER APL-UW TR 2001	
9. SPONSORING / MONITORING AGENCY NAME(S) AND ADDRESS(ES) Alaska Department of Fish and Game HQ Office P.O. Box 25526 Juneau, AK 99802-5526			10. SPONSORING / MONITORING AGENCY REPORT NUMBER	
11. SUPPLEMENTARY NOTES Approved for public release; distribution is unlimited.				
12a. DISTRIBUTION / AVAILABILITY STATEMENT Approved for public release; distribution is unlimited.			12b. DISTRIBUTION CODE	
13. ABSTRACT (Maximum 200 words)  During the summer of 1999, the Applied Physics Laboratory worked with the Alaska Department of Fish and Game, Biosonics Inc., and Hydroacoustics Technology Inc. to make underwater environmental acoustic measurements in Alaska's Kenai and Wood rivers. The goal of these measurements was to understand, and model, the sources and magnitude of background acoustic reverberation, defined as the average acoustic intensity versus time (range) delay in the absence of any scattering from fish. The background reverberation determines, in part, the minimum size class of fish detectable and the accuracy of fish-tracking and counting algorithms that exploit the complex phase of the fish echo. It is also necessary to establish rigorous detection probabilities for all fish size classes. This report summarizes the results and analysis of these measurements and presents environmental acoustic models that can be used to evaluate signal processing and fish-tracking algorithms.				
14. SUBJECT TERMS Sonar estimates of fish passage, acoustic detection of fish, reverberation, environmental acoustics.			15. NUMBER OF PAGES 35	
			16. PRICE CODE	
17. SECURITY CLASSIFICATION OF REPORT Unclassified	18. SECURITY CLASSIFICATION OF THIS PAGE Unclassified	19. SECURITY CLASSIFICATION OF ABSTRACT Unclassified	20. LIMITATION OF ABSTRACT \$AR	